THE ASTROPHYSICAL JOURNAL, 314:242–251, 1987 March 1

VELOCITY STRUCTURE OF STELLAR ATMOSPHERES: R SCUTI

DAVID MOZURKEWICH[1,2]
Wyoming Infrared Observatory, University of Wyoming, Laramie; and E. O. Hulburt Center for Space Research, Naval Research Laboratory
R. D. GEHRZ[2]
Wyoming Infrared Observatory, University of Wyoming, Laramie
K. H. HINKLE
National Optical Astronomy Observatory, Tucson
AND
D. L. LAMBERT
Department of Astronomy, University of Texas, Austin
Received 1986 April 10; accepted 1986 August 26

ABSTRACT

High-resolution ($\lambda/\Delta\lambda \approx 30{,}000$) 2 μm spectrograms were used to study the atmospheric motions of R Scuti, the brightest RV Tauri variable. The infrared atomic absorption lines are always single and trace out a continuous, repeatable pulsation with a mean velocity of 37 km s^{-1}, a net displacement of $R_{max} - R_{min} = 5 \times 10^{12}$ cm, and a period of about 142 days. Our observations are not consistent with the 70 day pulsation proposed to explain the visible spectrum by Preston in 1962.

Three molecules—CO, OH, H_2O—have been detected. The molecular line profiles reveal more complicated phenomena. Three absorption components and emission are present in the CO profiles on one spectrogram. CO has been observed falling toward the star at all phases. We propose that the molecular absorption forms higher in the star's atmosphere than the atomic absorption and invoke the Mira models published by Willson and Hill 1979 to explain the general features.

Emission components are usually present in both the atomic and the molecular lines. The atomic emission probably originates in a cool, extended envelope, whereas the molecular emission is attributed to a shock front.

Subject headings: shock waves — stars: emission-line — stars: individual — stars: pulsation — stars: RV Tauri variables

I. INTRODUCTION

The RV Tauri variables are a class of semiregular, pulsating, evolved stars characterized by alternating deep and shallow minima in their visible light curves. They consist of old disk and Population II stars. As a group, these stars have extensive amounts of circumstellar material, as indicated by a strong midinfrared excess (Gehrz 1972) and large visible polarization (Serkowski 1970; Henson, Kemp, and Kraus 1985). At maximum, the visible spectrum is characteristic of an F–G supergiant, but at minimum light, TiO absorption appears in some of the stars and can be strong enough to suggest a spectral class of M4. The stars appear not to undergo simple pulsations: the published velocity curves, as derived from metal lines in the visible, are discontinuous, there are multiple absorption components and emission is often present (Preston 1962, 1964; Baird 1982). In this paper we analyze ten 2 μm spectra of R Scuti, the brightest RV Tauri variable. This is the first analysis of high-resolution infrared spectra for an RV Tauri variable.

II. OBSERVATIONS

All data were taken between 1980 October and 1983 October using the 1.4 m Fourier transform spectrometer (FTS; Hall *et al.* 1979) on the Mayall 4 m telescope at KPNO, with resolutions of 0.1–0.15 cm^{-1}. A log of the observations is presented in Table 1. The spectra were apodized using the function I2 from Norton and Beer (1976). A calibration lamp and reference stars were observed during each observing session to determine the system response and telluric absorption as a function of wavenumber. The reference stars were not always observed at the same air mass as R Scuti. However, reasonable cancellation of the telluric features was obtained after adjusting the reference spectrogram to the appropriate air mass by assuming exponential extinction and a homogeneous atmosphere. Because misalignments of an FTS can cause frequency shifts mimicking a Doppler shift, the wavenumber scale was checked by measuring 49 telluric H_2O lines in each reference star spectrum. The positions of these lines agreed with the tabulation by Flaud *et. al.* (1977) to within 0.5 km s^{-1}. The velocities quoted in this paper should be free from systematic uncertainties to better than 1 km s^{-1}

Following the usual procedure for these stars, the measured pulsational velocities were not corrected for projection effects. Therefore, the pulsational velocities considered here should be regarded as lower limits. However, supergiants, such as R Scuti, should have stronger limb darkening than main-sequence stars, and consequently smaller projection effects. The correction is a factor of 1.4 for a main-sequence star.

Species identified in the 2 μm spectrum of R Scuti include H, Ti, Si, S, Ca, Na, Mg (Litzen 1964; Litzen and Verges 1976; Risberg 1967; Jakobsson 1966; Biémont 1976). The lines are from neutral atoms and have excitation energies from 1.7 to 8

[1] NRC-NRL Cooperative Research Associate.
[2] Visiting Astronomer, Kitt Peak National Observatory which is operated by the Association of Universities for Research in Astronomy, Inc., under contract with the National Science Foundation.

TABLE 1

LOG OF OBSERVATIONS

NUMBER	JD[a]	PHASE[b]	RESOLUTION (cm^{-1})	VELOCITIES[d] (km s^{-1})						
				Absorption					Emission	
				CO[c]		H_2O	OH	Atomic	CO	H_2O	Atomic
1.....	JD 4,542.5	0.65	0.15	49	...	...	...	27	...	...	42
2.....	JD 4,657.2	1.46	0.15	54	...	...	...	31	31	40	42
3.....	JD 4,926.6	3.35	0.13	42	61	43	...	41	24	...	38
4.....	JD 5,152.0	4.94	0.15	46	32	...	...	41	63	...	...
5.....	JD 5,279.0	5.84	0.15	52	26	...	...	28	49	40	47
6.....	JD 5,394.3	6.65	0.11	42	60[e]	...	51	27	35	...	40
7.....	JD 5,475.5	7.22	0.11	36	...	36	42	37	...	...	...
8.....	JD 5,490.1	7.32	0.11	37	...	37	43	36	...	...	...
9.....	JD 5,591.7	8.04	0.11	50	...	53	50	54	29	...	45
10.....	JD 5,621.5	8.25	0.11	60	...	55	60	43	...	...	...

[a] Julian dates are referenced 2,440,000.

[b] Photometric phase determined from phase = (JD − 4,450)/142, giving 0 phase at minimum light.

[c] The first column of CO lists the velocity of the component most prominent in the low-J lines. The rest of the components are listed in the second column.

[d] All velocities are heliocentric.

[e] A third CO component is at 23 km s^{-1}.

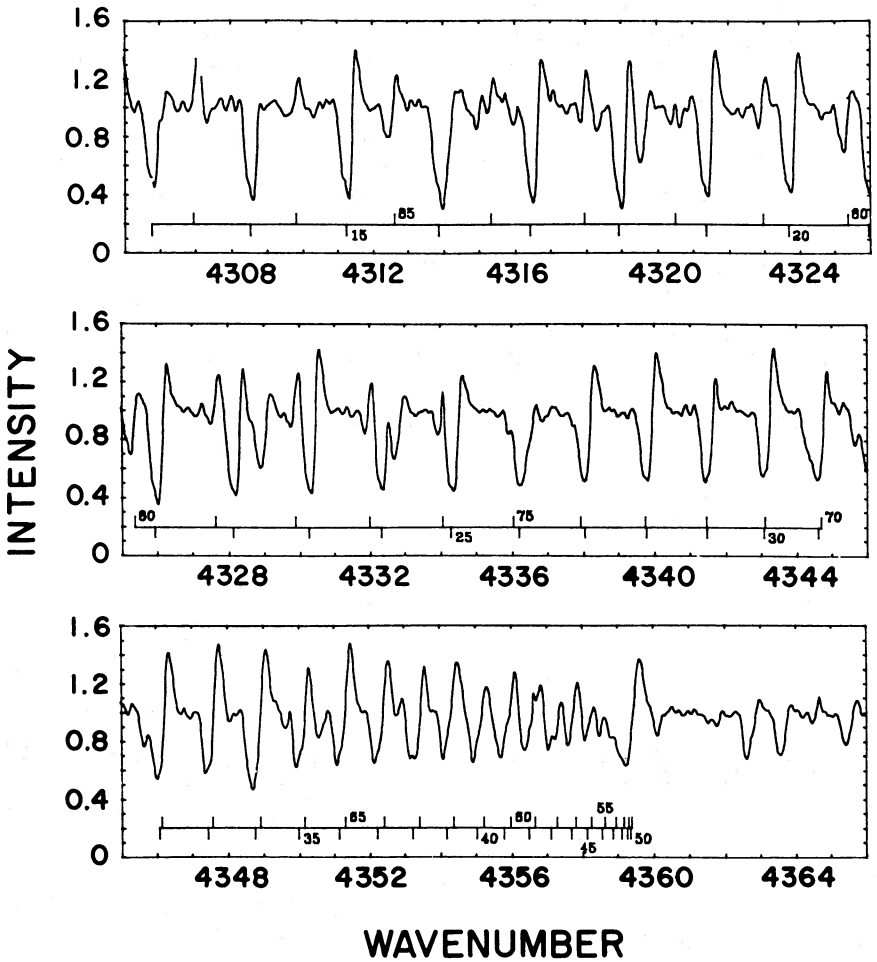

FIG. 1.—A segment of R Scuti's spectrum on JD 5,591 covering most of the unblended CO lines in the (2–0) band. The CO lines are marked and labeled with their J numbers. The lines with $J \gg 50$ are not present in this spectrogram. The unmarked absorption lines are from H_2O. All of the spectrograms shown in this paper have been corrected for absorption by Earth's atmosphere.

eV. These are the lines expected in a typical G supergiant. However, molecular lines dominate the spectrum at all phases and will occupy most of the discussion. Vibration-rotation transitions from the electronic ground states of three molecules have been identified. The first-overtone bands from CO (Kildal, Eng, and Ross 1974) were always present. Several of the spectra also cover the second-overtone bands, but none of these lines are present. However, the first-overtone OH bands (Maillard and Chauville 1976) are prominent on all of the spectrograms covering the appropriate spectral region. H_2O (Flaud, Camay-Peyret, and Maillard 1976) has been identified on eight of the 10 spectrograms. The lines can be quite strong. They represent the (001) → (000), (011) → (010), and (011) → (000) vibrational transitions.

The spectra will now be described in order of increasing phase. We follow the usual convention of having deep minimum light occur at 0 phase. The phase was determined from ϕ = (JD − JD 4,450)/142. This choice will be justified in § IV.

III. DESCRIPTION OF THE SPECTRUM

a) JD 5,591; ϕ = 0.04

A major portion of the *R* branch of the (2–0) band of CO is reproduced in Figure 1. The lowest excitation line shown is (2–0) *R*13 at 4306 cm^{-1}. The excitation energy of the lines increases toward higher wavenumbers, until the bandhead (*R*51) at 4360 cm^{-1} is reached and then the lines with $J > 51$ run toward lower wavenumber, overlapping the low-*J* lines until $J \approx 75$. Each line near the bandhead is a blend. For moderate optical depths and temperatures less than 5000 K, the contribution from the higher *J* component is negligible for $J > 65$–70. As a result, there are about 20 unblended lines with an excitation energy in the range from 0.05 to 0.25 eV. For brevity, we will refer to the $J < 25$ lines as the low-*J* lines, the $28 < J < 50$ as the mid-*J* lines, and the $J > 75$ lines as the high-*J* lines. The rest of the absorption lines in Figure 1 are due to stellar H_2O including the three prominent lines beyond the CO (2–0) bandhead.

The (3–1) band is similar to the (2–0) band, with a bandhead occurring at 4305 cm^{-1}. It overlaps the *P* branch ($J \rightarrow J$–1) as well as the $J < 13$ and $J > 87$ lines in the *R* branch of the (2–0) band. The 20 unblended lines have excitation energies between 0.3 and 0.7 eV.

Because of the close spacing of the energy levels, it is reasonable for several adjacent line profiles to be averaged to improve the signal-to-noise ratio. The averaged line profiles, for three sets of lines are shown in panel (*a*) of Figure 2. The absorption in the low-*J* lines is asymmetric, with a minimum at 45 km s^{-1}. As the energy increases, the profile becomes symmetric and the minimum shifts to 56 km s^{-1}. The simplest explanation for this behavior is to assume that the material responsible for the absorption at 45 km s^{-1} is cooler than the material at higher velocities.

The atomic lines are strong with absorption at 54 km s^{-1} and emission at 45 km s^{-1}.

b) JD 5,621; ϕ = 0.25

The atomic lines are strong and in absorption at 43 km s^{-1}. There is no definite atomic emission, nor emission in the high-*J* CO lines. The emission is weak but present on the blue wing of

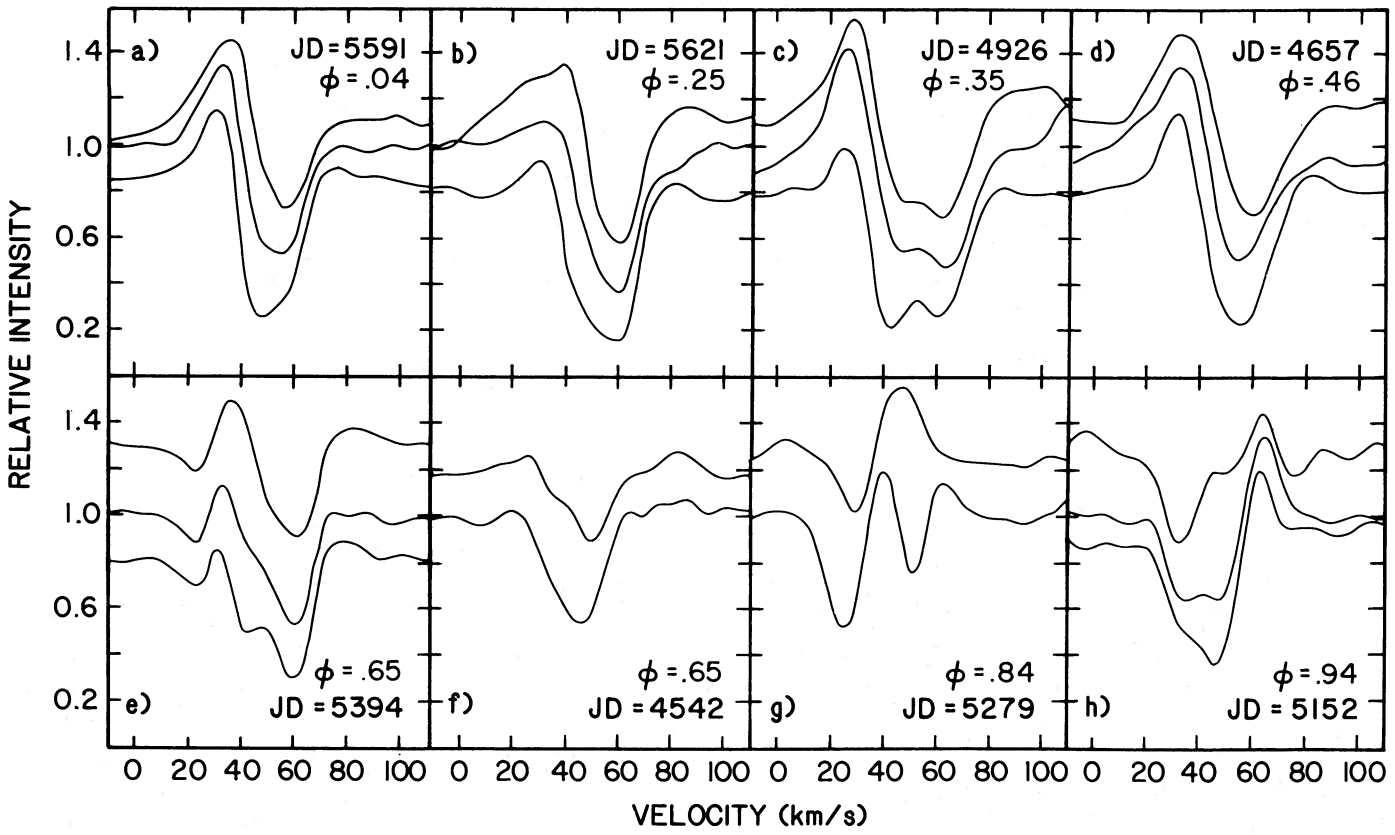

FIG. 2.—Averaged CO line profiles for eight of the spectrograms. In each panel, the lines increase in energy from the bottom to the top. They average 0.05, 0.2, and 0.4 eV. On JD 4,542, the energies are 0.1 and 0.4 eV. For JD 5,279, they are 0.5 and 1.7 eV.

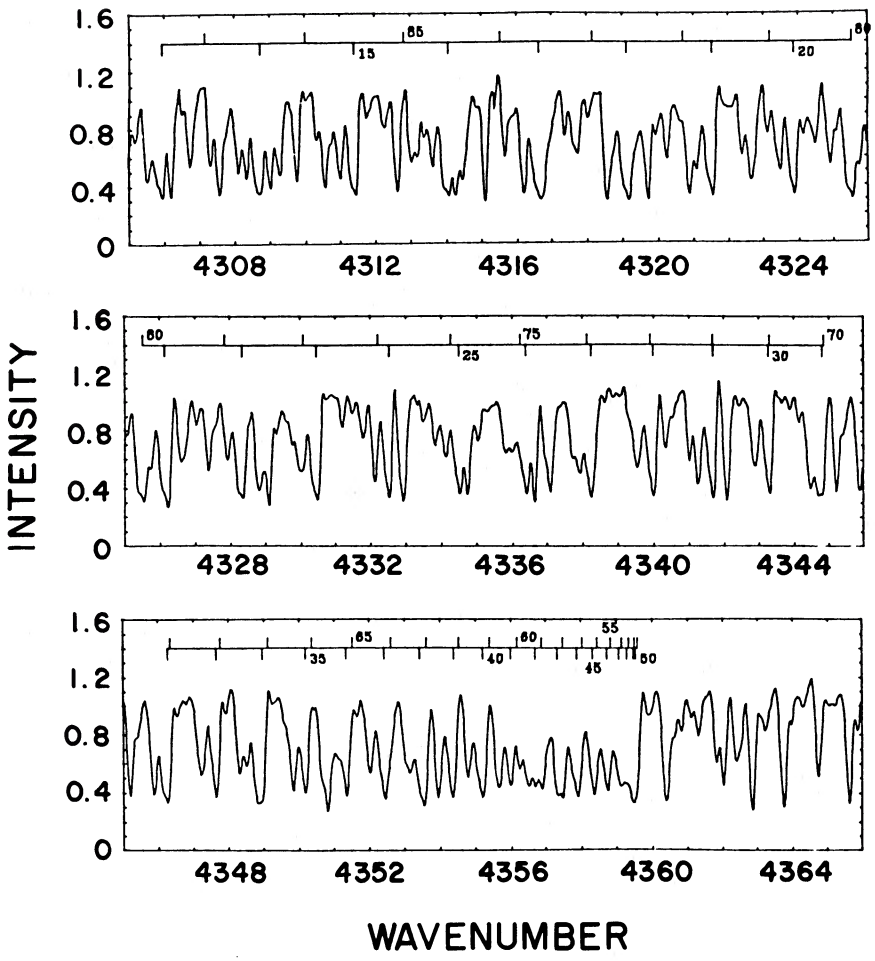

FIG. 3.—The same portion of the spectrogram shown in Fig. 1, but taken on JD 5,475. The CO lines are marked. The other lines are due to stellar H_2O. The spectrum on JD 5,490 is similar to this.

the low-J and mid-J CO lines. The average CO line profiles are shown in Figure 2, panel (*b*). The absorption is asymmetric, in the same sense as on JD 5,591, but now the 60 km s^{-1} component is deepest in all of the lines.

c) JD 5,475 and JD 5,490; $\phi = 0.22$ and 0.32

The spectrum on these two dates, 2 weeks apart, are similar but differ strikingly from the spectrum at $\phi = 0.25$ from the following cycle although they bracket it in phase. The entire spectrum is obscured by very strong H_2O absorption at 36 km s^{-1} on JD 5,475 (Fig. 3), and at 37 km s^{-1} on JD 5,490 with central depths >0.8. The strongest lines are those present in the other spectrograms. All water vapor lines in the laboratory line list (Flaud, Camy-Peyret, and Maillard 1976) have been identified in these spectrograms. In addition, there are still some unidentified lines. H_2O is the the most likely origin, since many satellite and hot bands should be present, but other species (e.g., CN) may also contribute. The CO lines are at the same velocity as the H_2O. The atomic lines are at 37 km s^{-1}, but are hard to identify because of the strong H_2O.

d) JD 4,926; $\phi = 0.35$

The H_2O does not dominate this spectrum but is present in absorption at 43 km s^{-1}. It is weaker than on any of the dates already discussed. The CO profiles now have two distinct minima. Assuming the minima are from two separate velocity components, their velocities are 42 and 61 km s^{-1}. Panel (*c*) of Figure 2 shows the averaged line profiles. In the low-excitation lines, the 42 km s^{-1} component is deepest. On higher excitation lines, this component weakens relative to the 61 km s^{-1} component. The atomic lines are in emission at 38 km s^{-1} and absorption at 41 km s^{-1}.

e) JD 4,657; $\phi = 0.46$

At this phase, the CO lines have returned to a simple inverse P Cygni profile with absorption at 54 km s^{-1} and emission at 31 km s^{-1} (panel [*d*] of Fig. 2). Again, the velocity of the absorption increases with the excitation energy. The H_2O is now in emission and is at 40 km s^{-1}, close to the velocity of the atomic emission (42 km s^{-1}) not the CO emission (31 km). These are the same H_2O lines found in absorption at other phases.

f) JD 4,542 and JD 5,394; $\phi = 0.65$

The spectrogram on JD 5,394 exhibits the most complex CO profiles observed. The 42 km s^{-1} component is flanked by components at 60 km s^{-1} and 23 km s^{-1}. The averaged line profiles are shown in panel (*e*) of Figure 2. The lowest excita-

tion lines show no definite emission. In the higher excitation lines, the 42 km s^{-1} absorption disappears, while emission at 35 km s^{-1} becomes visible.

The JD 4,542 spectrogram (panel [*f*] of Fig. 2) was taken at the same phase. A single CO absorption is at 49 km s^{-1} in the low-excitation lines, but shifts to 52 km s^{-1} in the (3–1) band. By associating the component present in the (3–1) band with the highest velocity component present on JD 5,394, we can estimate that the CO velocity varies by about 8 km s^{-1} between cycles.

There is no H_2O present in either spectrogram. The atomic lines have similar velocities on the two spectrograms.

g) JD 5,279; $\phi = 0.84$

The averaged CO line profiles from the spectrogram taken on JD 5,279 are shown in panel (*g*) of Figure 2. This spectrogram has the strongest CO emission, at 49 km s^{-1}. The emission is clearly overlain by a cool absorption feature at 52 km s^{-1}. The warm CO absorption, at 26 km s^{-1}, as well as the CO emission, are very strong and extend into the high-*J* lines. The atomic lines again show both emission and absorption, with the highest excitation lines in absorption at 28 km s^{-1} and the lowest excitation lines in emission at 47 km s^{-1}. The H_2O is in emission at 40 km s^{-1}.

h) JD 5,152; $\phi = 0.94$

This spectrogram is short, extending only from 4000 to 4500 cm^{-1}. As a result, fewer atomic lines are present. There is no definite atomic emission in this spectrogram. The atomic absorption velocity is 41 km s^{-1}. The CO lines on JD 5,152 show both emission and absorption. The emission is at 63 km s^{-1}. This spectrogram also shows emission in the high-*J* lines at 54 km s^{-1}. The line profiles are shown in panel (*h*) of Figure 2. The lowest excitation lines are asymmetric with a minimum at 46 km s^{-1}. The mid-*J* lines have two distinct minima. The lines in the (3–1) band have a single minimum at 32 km s^{-1}. No H_2O lines were detected in this spectrogram.

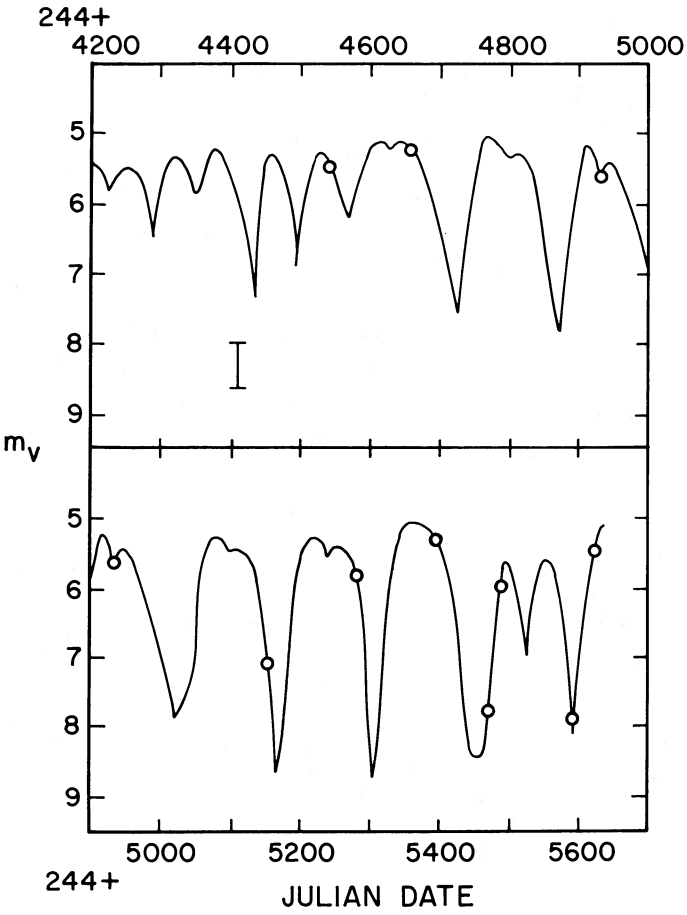

FIG. 4.—AAVSO light curve for R Scuti. The vertical bar indicates the peak-to-peak scatter on the light curve. The 2 μm spectra discussed here were taken on the dates marked with circles.

IV. DISCUSSION

When we ordered the observations in the previous section by phase, we implicitly assumed that combining the observations from several cycles correctly describes the variation during a single pulsation. In the rest of this section, we will show that this assumption is consistent with our data, despite the irregularity of the visible light curve (Fig. 4). Since the light curve of R Scuti is one of the least regular of all of the RV Tauri variables, a discussion of why this assumption is valid is warranted.

Empirically, the velocity curves of RV Tauri variables are more stable than the light curves. Preston (1964) successfully constructed a radial velocity curve for a similar star U Mon from data spanning 800 days. All of the data was folded onto one 46 day period. This is apparently also the case for other cool, luminous stars. For example, the 2 μm spectra of Mira variables presented by Hinkle (1978) and Hinkle, Hall, and Ridgway (1982) are stable over more than one period, despite the irregularity seen in the visible.

Perhaps we can understand this when we realize that the material above the photosphere in these stars is at a temperature where molecules are beginning to form. Thus small changes in temperature can result in large changes in the opacity. Variations in the visible light curve, especially changes in the depth or width of the minima, may reflect small temperature changes in the upper atmosphere and bear little relationship to conditions at any appreciable depth in the star. At 3000 K, the H^- opacity decreases by a factor of 5 from 5000 Å to 2 μm. Thus, the 2 μm spectra we present here probe deeper layers of the star, enhancing the contrast between the irregular light curve and the regular atomic absorption velocity curve. The CO lines form higher in the atmosphere in a region more affected by the opacity variations. These lines may show larger variations between periods.

There is some disagreement about R Scuti's period. Recently quoted values range from 140 days (e.g., Howell, Bopp, and Noah 1983) to 144 days (Luck 1981). To complicate the picture, the light curves of RV Tauri variables are known to undergo phase shifts, making it impossible to improve the period by comparing the times of widely separated minima (e.g., DuPuy 1973; Klyus 1981). We measured the times of deep minimum from the AAVSO light curve (Fig. 4; Mattei 1983). A least-squares fit to these times yields a period of 145 days. Next, we determined a period from the atomic absorption velocities. Due to their higher excitation energies, these lines should form in the deep photosphere and have more reproducible velocities than the molecular lines. A period of 140 days gives the smoothest curve and least scatter in the atomic absorption velocities. We chose a compromise period of 142 days.

a) Atomic Absorption

The atomic absorption velocities are based on the highest excitation lines present in the spectrum which where almost exclusively free from emission. The velocity curve generated from these lines is shown in the upper panel of Figure 5. It exhibits a single, continuous variation. The maximum velocity occurs just after minimum light. The velocity curve was integrated to yield a mean velocity of 37 km s^{-1} and net displacement ($R_{max} - R_{min}$) of 5×10^{12} cm. There is no resemblance to the velocity curve of R Scuti generated from the visible spectrum (Preston 1962). The velocity curve is discontinuous, and repeats with one-half the period. In the light of this difference, we tried periods around 70 days, but none of those gave a reproducible velocity curve.

If the atomic absorption lines form in the same layer of material at all phases, we can estimate the radius of the star by assuming that the maximum inward acceleration occurs while the layer is in free fall. This estimate will be too large if the pressure decreases outward and the pressure gradient is large enough to significantly decrease the effective gravity. Assuming a mass of 0.6 $M_\odot$ (Gingold 1974), the observed acceleration (1.1 cm s^{-2}) gives a radius of 8.5×10^{12} cm. Adopting this as the mean, the radius changes by almost a factor of 2, from $6. \times 10^{12}$ to 1.1×10^{13} cm, during the pulsation. A distance of 330 pc was adopted for R Scuti. This was determined from the period—luminosity relationship: $M_v = -5.3 + 0.021P$ (days) (DuPuy 1973; DuPuy and Barnes 1975), using a period of 142 days, a mean visual magnitude of 5.8 and 1.5 mag of extinction per kiloparsec. Another estimate for the star's radius can be determined from the magnitude of the star and the effective temperature at that wavelength. Except at minimum light, the 2 μm magnitude of R Scuti is relatively constant at 2.3. It is difficult to chose an appropriate temperature. Temperature estimates are as high as Luck's (1981) $T_{eff} = 4000$ K, determined from visible spectroscopy, to $T_{ex} = 3500$ K determined from a differential curve of growth of Fe lines in the visible spectrum (Preston 1962). Even lower temperatures may be inferred from the presence of strong TiO in the visible spectrum and H_2O absorption in the 2 μm spectrum at some phases. Fortunately, the radius of the star is only weakly dependent on the temperature. A temperature of 4400 K gives a radius of $5. \times 10^{12}$ cm. To obtain a radius of $1. \times 10^{13}$ cm, the temperature has to be lowered to 2300 K. Since this radius is in agreement with the kinematic result of the previous paragraph, we feel that the atomic velocities reflect actual motion of a mass element in the star. For the rest of this paper, we will refer to the region where the atomic absorption lines form as the photosphere.

What is responsible for the differences between the visible velocity curve and the 2 μm curve? The 2 μm curve represents conditions deeper in the star, since it was generated from higher excitation lines (6–8 eV vs. 1.5–2.5 eV) in a part of the spectrum where the continuum opacity, from H^-, is five times

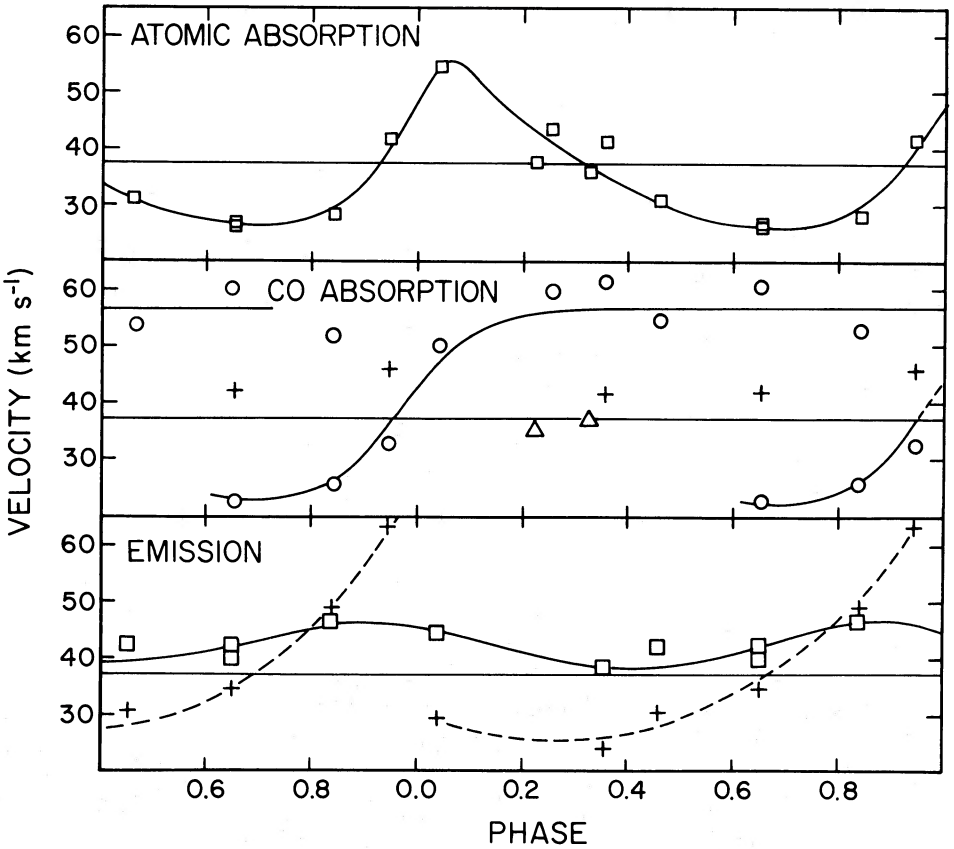

FIG. 5.—Velocity as a function of phase for atomic absorption lines (*upper panel*), CO absorption (*middle panel*), and emission (*lower panel*). The curve is repeated over 1.6 periods for clarity. The velocities are heliocentric, with the mean velocity of the atomic absorption lines occurring at 37 km s^{-1}. Primary minimum occurs at phase 0. Squares denote atomic lines. All other symbols refer to CO. In the middle panel, the plus sign denotes the coolest component. The triangles indicate the CO velocities on the two dates with very strong H_2O absorption (JD 5,475 and JD 5,490).

weaker than in the visible. If a shock wave travels outward from its origin just above the photosphere, the 2 μm lines will never be doubled; the visible lines will be doubled when the shock is in the region sampled by those lines. However, in order to explain the shorter period of the visible lines, two shock waves must form during each pulsation of the photosphere. In addition, we argue in § IV*b* that the CO lines are formed in this region. They show no evidence of a 70 day period.

The AAVSO light curve suggests an alternative. Preston's observations were made when the light variations were similar to the first three minima in Figure 4. The visible light decreased 1 to 1.5 mag at deep minimum and about half of that at secondary minimum. During our observations, the primary minima were much deeper (more than 3 mag), and the secondary minima were almost, if not completely absent. Both the light and velocity curves suggest that R Scuti was not oscillating with the short period during our observations. If these periods correspond to the fundamental and an overtone (e.g., Takeuti and Peterson 1983), then the overtone was not strongly excited during our observations. A radial pulsation in a supergiant does not extend into the star's core (e.g., Cox 1980). Most of the energy in the first overtone pulsation is concentrated in the outer 15% of the mass. Since R Scuti's radius changes by a factor of 2 during a pulsation, it is not unreasonable to expect large changes in the relative strength of the overtone.

b) Carbon Monoxide Absorption

The CO velocities are shown in the middle panel of Figure 5. Because of the vast number of components present, they are subdivided into groups. The velocity components most prominent in the low-J lines are designated by plus signs in the figure and will be referred to as "cool" components. The "warm" components dominate the absorption in the mid-J lines and in the (3–1) branch. They are denoted with circles. Triangles designate the CO velocities on the two spectra with very strong H_2O lines (JD 5,475 and JD 5,490).

Warm CO is present near the photospheric velocity from phase 0.6 to 0.04. This is reasonable, since these phases bracket the maximum photospheric radius, and presumably minimum photospheric temperature. These CO velocities average about 3 km s^{-1} smaller (faster outflow) than the photospheric velocity. From phase 0.04 until 0.65 there is a warm component between 55 and 60 km s^{-1}. This range is roughly the period-to-period variation seen at phase 0.65. The presence of emission near this velocity at phases 0.84 and 0.94 prevents us from determining if this component is present at all phases. The rest of the CO components are cool and have velocities from 40 to 50 km s^{-1}.

If the 60 km s^{-1} component represents a layer of material falling toward the star, then it will travel about 3×10^{13} cm during one period and must be quite distant from the star to remain at constant velocity. The situation is not improved if it is assumed to be a continuation of the CO component present at the photospheric velocity from phase 0.65 to 1.0. In this case, the material falls 1.6×10^{13} cm toward the star in one period. This material, then, could not originate in the photosphere as suggested by the similarity of velocities.

An interpretation of these observations seems to be contained in the shock wave models suggested by Willson and Hill (1979) for Mira variables. A shock wave propagates out from the photosphere through a tenuous upper atmosphere. The highest inward velocity is just above of the shock. The velocity decreases outward from there (Fig. 6*a*). Numerical calculations (Hill and Willson 1979) indicate that as the shock propagates outwards the maximum inward velocity remains roughly constant. Material is always falling toward the star at the velocity, but it is different material at different phases.

In these models, a mass element passing through the shock receives an upward boost in velocity. During the rest of the period, gravity accelerates the mass element toward the star. If the impuse from the shock equals the momentum loss during the rest of the period, the mass element will be suspended (Fig. 6*b*), neither escaping from the star nor falling back to the photosphere. This will occur if the time, P_0, for the mass element to travel outward and then fall to the height where it originally passed through the shock is equal to the time between shocks, P (the period of the pulsation). At larger radii, P_0 increases, the particle hits the shock at progressively larger radii, and eventually escapes from the star.

To suspend material above the photosphere, P_0 must be equal to P. In addition, the outward velocity of the shock must equal the inward velocity of the material just prior to encountering the shock. A period of 142 days, a stellar mass of 0.6 $M_\odot$, and an outward-shock velocity of 20 km s^{-1}, give a radius of 1.2×10^{13} cm. This is close to our estimated maximum radius of the photosphere: it would not be surprising to find a substantial amount of material in this region. This material can persist by itself, or it may feed nearly continuous mass loss and in turn be fed every period by material from the photosphere. Alternatively, it may occasionally be filled or emptied by an unusually strong shock wave.

This entire shock-dominated region is optically thin in the continuum at all phases, since we can see atomic absorption lines from the photosphere. Material should be present not only directly above the shock at 60 km s^{-1}, but also higher up where it will have lower velocities. A reexamination of Figure 2 indicates that this indeed occurs. The full width of the CO absorption often exceed 20 km s^{-1}. At several phases, these broad lines have a second minimum at $\sim$40 km s^{-1} (near the systemic velocity). This second component can be understood since material accelerated upward by the shock spends most of its time with a velocity near the systemic velocity.

We can now explain all of the CO absorption. The "warm" component at 55–60 km s^{-1} forms in the material immediately above the shock. The "cool" components from 40 to 50 km s^{-1} form in cooler material further above the shock. Finally, the "warm" component at less than 40 km s^{-1} ($0.6 < \phi < 1.0$) is assigned to the photosphere.

c) Emission

A clue to the origin of the atomic emission lines is shown in Figure 7. The systematic decrease of emission-line strength with energy is present on all spectrograms where the atomic lines show both emission and absorption. The implication is that the emission originates in a region which is cooler than, and hence extended relative to the photosphere.

The atomic emission velocities are marked with boxes in the bottom panel of Figure 5. These atomic velocities were determined mainly from several Ti I lines (1.7 eV). They show a small, sinusoidal variation with half amplitude of 4 km s^{-1} and maximum velocity occurring at maximum photospheric radius. The mean atomic emission velocity, 43 km s^{-1}, differs from the mean atomic absorption velocity, 37 km s^{-1}. If the emission originates in an extended envelope, the mean velocity

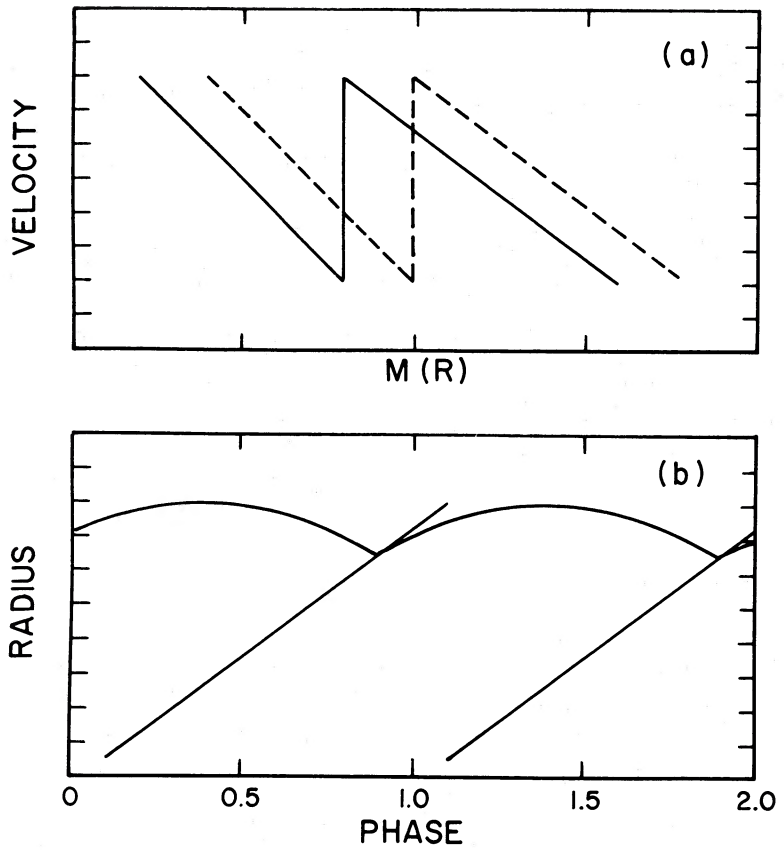

FIG. 6.—(*a*) The velocity structure of R Scuti's atmosphere (*solid line*) proposed to account for the CO velocities. The discontinuity is caused by a shock wave. At a later time (*dashed line*) all of the material has accelerated toward the star due to gravity, but the shock has also moved outward. This accounts for the constant maximum inward velocity observed. (*b*) The trajectory of a mass element suspended above the star by the shock. These figures are patterned after Figs. 1 and 2 of Hill and Willson (1979).

should be close to the center-of-mass velocity of the system. It can be biased to larger velocities only if the envelope is contracting, since the material with the lowest velocity along the line-of-sight is hidden behind the star. In this case, the maximum bias will occur at maximum photospheric radius, as observed. We attribute the atomic emission to an extended envelope surrounding the star.

The velocity of the high-J CO emission, when present, usually agrees with the atomic emission velocity and is attributed to the same origin. The velocity of the low-J emission does not (denoted by plus signs in the lower panel of Fig. 5). The CO line profiles for JD 5279 clearly show that the cool absorption component originates above the emission. This restricts the CO emission, at least on this date, to the region between the photosphere and the layer of CO immediately above the shock. We therefore attribute the low-J CO emission to a hot region immediately below and heated by the shock. Hill and Willson (1979) find that the shock forms while the photosphere is still contracting, but decelerating (between phases 0. and 0.3). The onset of outward-moving CO emission at phase 0.04 is consistent with the shock interpretation.

Baird (1984) tried to apply a modification of the Wilson and Hill shock wave model to another RV Tauri variable, AC Her. There, a second, deeper shock is also visible and is used to explain several high-velocity lines in his data. The photosphere driving the shocks is still deeper and is hidden from view. There are no features in our spectra which require the existence of this second shock in R Scuti.

d) Water and Hydroxyl

The water features are difficult to explain. The five spectra taken between phases 0.04 and 0.46 show H_2O in absorption within 2 km s^{-1} of a CO absorption component. During the rest of the pulsation, it is either in emission or absent. When it is in emission, its velocity is closer to the atomic emission than to the CO emission. Emission and absorption components are never present in the same spectrogram, and similar lines are present in both emission and absorption.

The description in the previous paragraph may be misleading since there are large cycle-to-cycle variations in the velocity and strength of the H_2O absorption. This is dramatically illustrated by the two spectrograms JD 5,475 (Fig. 3) and JD 5,490. The central depths of the strongest lines have increased to > 0.8, and a plethora of weaker lines obscure the CO bands as well as the continuum through most of the spectrum. This should be contrasted with the more typical spectrogram in Figure 1. The velocity of these lines suggests an association with the photosphere. However, chemical equilibrium calculations for oxygen-rich stars (Goon and Auman 1970; Tsuji 1964) indicate that H_2O does not become abundant until the temperature drops to 2200–2400 K. At this phase the photosphere has its minimum radius and presumably is close to the hottest part of its pulsation. The photospheric temperature would have to drop 1000 K to 2000 K to allow for the formation of a significant amount of H_2O. A circumstellar origin of the lines is more likely, since the central depths are consistent

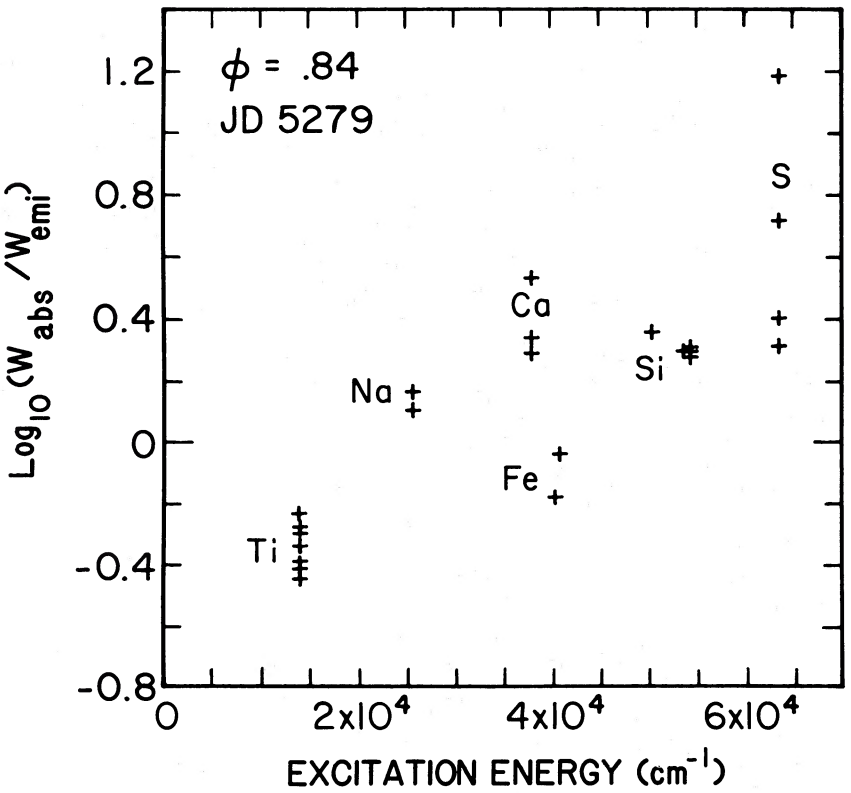

FIG. 7.—The ratio of equivalent widths for the atomic absorption and emission lines. Emission dominates the low excitation lines of Ti I, while absorption is dominant in the highest excitation lines. This trend implies that the emission originates in a region cooler than, and hence extended relative to, the photosphere. Similar trends are present in all of the spectrograms. We attribute the origin of this emission to an extended envelope surrounding the star.

with a layer of material cool enough to form water overlying a 3500–4000 K photosphere.

Since H_2O associates rapidly when the temperature drops below about 2400 K, we cannot conclusively determine whether the formation of the water lines indicate an increase in the amount of circumstellar material or merely a small drop in its temperature. The former possibility seems more likely, since the H_2O lines are accompanied by strong CO absorption at the same velocity. There is no evidence for CO at this velocity at the same phase during the following cycle (Fig. 2*b*).

OH is present in absorption on all five spectrograms covering the appropriate spectral region. A determination of their behavior as a function of phase is not possible since only one spectrum was obtained outside the phase range 0.04–0.46. All of the velocities are consistent with an origin in the material above the shock.

V. SUMMARY

Spectroscopy at 2 μm provides a wealth of information about the kinematics of cool stellar atmospheres. Our results for R Scuti are summarized below:

1. The period of R Scuti, determined from the atomic absorption lines, is 142 days, not 70 days as proposed to explain the visible spectrum. The infrared atomic absorption lines trace out a continuous, repeatable velocity curve which is interpreted as the radial pulsation of the star. The mean velocity is 37 km s^{-1} and the net displacement during a cycle is $R_{max} - R_{min} = 5 \times 10^{12}$ cm.

2. The CO lines form in the cooler, upper atmosphere. The dominant feature is material falling toward the star at about 20 km s^{-1}. The region is supported by a shock wave which passes through it once each pulsation. Material heated by the shock is responsible for the formation of the CO emission lines.

3. Surrounding the star is an extended envelope where the atomic emission lines form.

R Scuti's atmosphere has been well explained, qualitatively, using the shock wave models of Hill and Willson (1979). However, a few troublesome features remain. The assignment of the atomic emission to an extended envelope is weak, because of difficulties in explaining its velocity. Why does the high-excitation CO emission originate in the extended envelope when the lower excitation lines have been attributed to the shock? Finally, an understanding of the differences between the visible and IR spectra awaits simultaneous observations at both wavelengths.

We acknowledge the AAVSO observational data sent to us by the director, Janet A. Mattei. Infrared astronomy at the University of Wyoming is supported by the NSF, the USAF, and the state of Wyoming. D. L. L. acknowledges the partial support of the NSF (grant AST 83-16635).

REFERENCES

Baird, S. R. 1982, *Pub. A.S.P.*, **94**, 850.
———. 1984, *Pub. A.S.P.*, **96**, 72.
Biémont, E. 1976, *Astr. Ap. Suppl.*, **26**, 89.
Cox, J. P. 1980, *Theory of Stellar Pulsation* (Princeton: Princeton University Press).
DuPuy, D. L. 1973, *Ap. J.*, **185**, 597.

DuPuy, D. L., and Barnes, T. G. 1975, *Ap. J.*, **200**, 364.
Flaud, J.-M., Camy-Peyret, C., and Maillard, J. P. 1976, *Mol. Phys.*, **32**, 499.
Flaud, J.-M., Camy-Peyret, C., Maillard, J. P., and Guelachvilli, G. 1977, *J. Molec. Spectrosc.*, **65**, 219.
Gehrz, R. D. 1972, *Ap. J.*, **178**, 715.
Gingold, R. A. 1974, *Ap. J.*, **193**, 177.
Goon, G., and Auman, J. R. 1970, **161**, 533.
Hall, D. N. B., Ridgway, S., Bell, E. A., and Yarborough, J. M. 1979, *Proc. Soc. Photo-Opt. Instr. Eng.*, **172**, 121.
Henson, G. D., Kemp, J. C., and Kraus, D. J. 1985, *Pub. A.S.P.*, **97**, 1192.
Hill, S. J., and Willson, L. A. 1979, *Ap. J.*, **229**, 1029.
Hinkle, K. H. 1978, *Ap. J.*, **220**, 210.
Hinkle, K. H., Hall, D. N. B., and Ridgway, S. T. 1982, *Ap. J.*, **252**, 687.
Howell, S. B., Bopp, B. W., and Noah, P. V. 1983, *Publ. A.S.P.*, **95**, 762.
Jakobsson, L. R. 1966, *Ark. Fys.*, **34**, 19.
Kildal, H., Eng, R. S., and Ross, A. H. M. 1974, *J. Molec. Spectrosc.*, **53**, 479.
Kylus, I. A. 1981, *Soviet Astr.*, **25**, 207.
Litzen, U. 1964, *Ark. Fys.*, **28**, 239.
Litzen, U., and Verges, J. 1976, *Phys. Scripta*, **13**, 240.
Luck, R. E. 1981, *Pub. A.S.P.*, **93**, 211.
Maillard, J. P., and Chauville, J. 1976, *J. Molec. Spectrosc.*, **63**, 120.
Mattei, J. A. 1983, private communication.
Norton, R. H., and Beer, R. 1976, *J. Opt. Soc. Am.*, **66**, 157.
Preston, G. W. 1962, *Ap. J.*, **136**, 866.
———. 1964, *Ap. J.*, **140**, 173.
Risberg, G. 1967, *Ark.* Fys. **37**, 231.
Serkowski, K. 1970, *Ap. J.*, **160**, 1107.
Takeuti, M., and Petersen, J. O. 1983, *Astr. Ap.*, **117**, 352.
Tsuji, T. 1964, *Ann. Tokyo Obs.*, Ser. 2, **9**, 1.
Willson, L. A., and Hill, S. J. 1979, *Ap. J.*, **228**, 854.

R. D. GEHRZ: Department of Astronomy, The University of Minnesota, 116 Church Street, S.E., Minneapolis, MN 55455

K. H. HINKLE: National Optical Astronomy Observatory, Box 26732, Tucson, AZ 85726

D. L. LAMBERT: Department of Astronomy, University of Texas at Austin, Austin, TX 78712

DAVID MOZURKEWICH: Code 4138M, Space Science Division, Naval Research Laboratory, Washington, DC 20375-5000